Supporting Information

Hydrophobic Pores in a Calcium-Based MOF Enable One-Step Ethylene Purification from $C_2H_2/CO_2/C_2H_4$ Mixtures

Shanshan Mao, Jiafeng Miao, Kang Zhou, Li Yin, Fu-An Guo, Xiuze Hei and Hao Wang**

Hoffmann Institute of Advanced Materials, Shenzhen Polytechnic University, 7098 Liuxian Blvd., Nanshan, Shenzhen 518055, Guangdong, PR China

1. Experimental section

1.1. Material and General characterization

All reagents were obtained from commercial sources and used without additional purification. Among them, $CaCl_2$ (CAS: 10043-52-4) was purchased from Macklin; 1,3,6,8-Tetra(2-methyl-4-carboxyphenyl)pyrene (CAS: 2982238-30-0 was purchased from Nanchang Chouhe Pharmaceutical Technology Co., Ltd.; 95% ethanol (CAS: 64-17-5) was purchased from Aladdin;

Single-crystal X-ray diffraction (SCXRD) data were collected on a Bruker D8 VENTURE diffractometer equipped with a PHOTON II CPAD detector and a Ga-target Liquid METALJET D2 PLUS X-ray source (λ = 1.34139 Å). Structural determination was carried out using SHELXT (version 2018/2), and the refinement was performed by full-matrix least-squares methods with SHELXL (version 2018/3) through the OLEX2 graphical interface. Powder X-ray diffraction (PXRD) patterns were acquired on a Bruker D8 Advance diffractometer employing Cu-Kα radiation (λ = 1.5418 Å) within the 2θ range of 3–40°, at a scan rate of 5° min^{-1} and an operating power of 40 kV/40 mA. Thermogravimetric analysis (TGA) was conducted under a nitrogen atmosphere using a TGA 550 thermal analyzer (TA Instruments) with a heating rate of 10 °C min^{-1}. Single-component gas adsorption isotherms were measured on an automated volumetric adsorption apparatus. (BSD-660). The sample of Ca-lp-3 was degassed at 120 ℃ for 5 h under ultrahigh vacuum prior to data collection for CO_2, C_2H_2 and C_2H_4 at 273 and 298 K.

1.2. Synthesis

Synthesis of HIAM-204: Calcium chloride (60 mg) and the ligand 1,3,6,8-tetrakis(2-methyl-4-carboxyphenyl)pyrene (H_4TCMPP, 40 mg) were added to 5 mL of 95% ethanol solution. The solution was homogenized by sonication and then transferred to a 20 mL Teflon-lined stainless steel autoclave. The autoclave was heated in a 120°C oven for 3 days. Yellow rod-shaped crystals were obtained. The synthesized HIAM-

204 was collected by filtration and washed several times with fresh ethanol. Lastly, the activated sample was then activated at 393 K under dynamic vacuum for 5 hours.

1.3. Multicomponent column breakthrough tests

Breakthrough experiments were performed using an automated mixed-gas breakthrough system (BSD-MAB). A total of 0.4355 g of adsorbent was packed into a stainless-steel column with an inner diameter of 6 mm and a length of 80 mm. Prior to testing, the sample was activated at 393 K for 5 h under a helium flow of 10 mL min^{-1}. After cooling to 298 K, the helium stream was switched off, and a ternary mixed feed gas was introduced into the column at a total flow rate of 5/2 mL min^{-1}. The composition of the effluent gas was continuously monitored using a mass spectrometer. The C_2H_4 purity productivity was calculated by the following method: the gas breakthrough gas amount (qi) was calculated by integrating the breakthrough curve f(t) as following equation.

$$Q_{\mathrm{i}} = \frac{C_{\mathrm{i}} V}{\mathrm{m}} \times \int_0^{\mathrm{t}} \left(1 - \frac{F}{F_0}\right) dt \tag{1}$$

Here Q_i is the dynamic adsorption capacity of gas i (cm^3 g^{-1}), C_i is the feed gas concentration, V is the volumetric feed flow rate (cm^3 min^{-1}), t is the adsorption time (min), F_0 and F are the inlet and outlet gas molar flow rates, and m is the mass of the adsorbent (g). And then the purity (c) of breakthrough gas was calculated by the following equation.

$$\frac{q_{C2H2}}{q_{C2H2} + q_{CO2}} \tag{2}$$

1.3. IAST selectivity calculations for binary gas mixtures

The ideal adsorbed solution theory (IAST) was employed to predict the adsorption behavior of binary gas mixtures based on experimentally obtained single-component isotherms. The adsorption isotherms of HIAM-204 were fitted using the dual-site

Langmuir–Freundlich (DSLF) model, which can be expressed as follows:

$$q = \frac{q_{A,sat} * b_A * p^{v_A}}{1 + b_A * p^{v_A}} + \frac{q_{B,sat} * b_B * p^{v_B}}{1 + b_B * p^{v_B}} \quad (3)$$

with T-dependent parameters b_A, and b_B

$$b_A = b_{A0} \exp\left(\frac{E_A}{RT}\right); \quad b_b = b_{B0} \exp\left(\frac{E_B}{RT}\right) \quad (4)$$

Here, q denotes the adsorption amount of the adsorbent (mol/kg); $q_{a,sat}$ and $q_{\beta,sat}$ correspond to the saturated adsorption capacities at sites A and B, respectively. b_a and b_β are the affinity constants for the adsorbate at sites A and B, respectively, while p represents the total equilibrium pressure of the bulk gas. v_a and v_β are the Freundlich exponents associated with adsorption sites A and B, respectively.The IAST selectivity is defined by:

The adsorption selectivity for the mixture CO_2/C_2H_4 and C_2H_2/CO_2 is defined by

$$S_{ads} = \frac{x_1 / x_2}{y_1 / y_2} \quad (5)$$

Where q_1 and q_2 are the amounts of CO_2, C_2H_2, and C_2H_4 adsorbed on the sample under equilibrium conditions, typically expressed in mmol/g; y_1 and y_2 are the corresponding mole fractions of the mixture in the gas phase. The IAST adsorption selectivities were calculated for mixtures of CO_2/C_2H_4 (CO_2/C_2H_4 = 50:50 and 10:90 v/v) and C_2H_2/C_2H_4 (C_2H_2/C_2H_4 = 50:50 and 10:90 v/v) at 298 K and a total pressure of 101 kPa, with mole fractions y1 = 0.5/0.1 and y2 = 1-y1 = 0.5/0.9.

1.4. DFT calculations

In this study, all calculations were conducted using the spin-unrestricted density functional theory (DFT) approach as implemented in the DMol³ and Sorption modules of the Materials Studio package [1]. Electron exchange and correlation were treated within the generalized gradient approximation (GGA) using the Perdew–Burke–Ernzerhof (PBE) functional, and the double numerical plus polarization (DNP) basis

set was employed [2]. A smearing of 0.005 Ha was applied to the orbital occupations in all calculations. The convergence criteria were set to 2.0×10^{-5} Ha for energy change, 0.004 Ha $Å^{-1}$ for maximum force, and 0.005 Å for maximum displacement. Brillouin-zone integrations were performed using a 3 × 3 × 1 Monkhorst–Pack k-point grid [3]. All electron density maps were generated using the Sorption module with the COMPASS II force field. Van der Waals and Coulomb interactions were treated using the atom-based method and Ewald summation, respectively, with a cutoff distance of 12.5 Å. The simulations were conducted at a temperature of 323 K and a pressure of 100 kPa. The binding energy (ΔE) was calculated as

$$\Delta E_{ads} = E_{*gas} - E_{*} - E_{gas} \quad (8)$$

where E_{*gas}, E_{*}, and E_{gas} the energies of HIAM-204 adsorbed with molecule, isolated HIAM-204, and molecule, respectively.

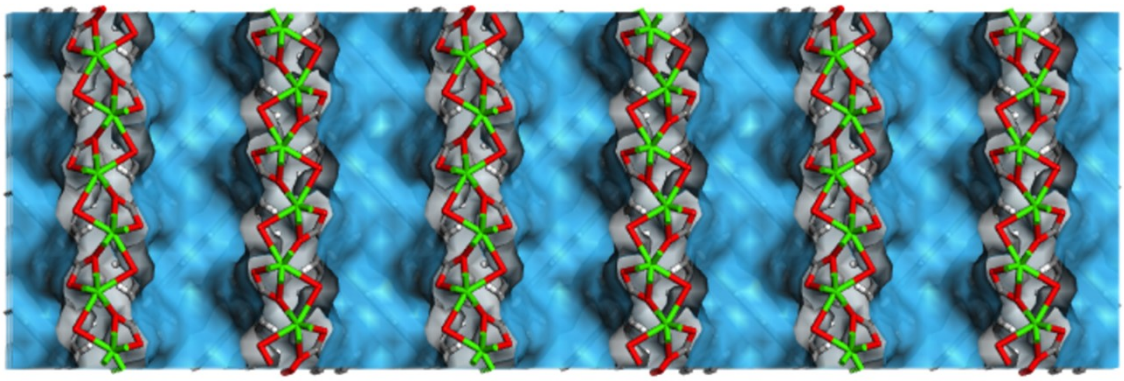

Figure S1. View for 1D Ca chain in the crystal structure of HIAM-204.

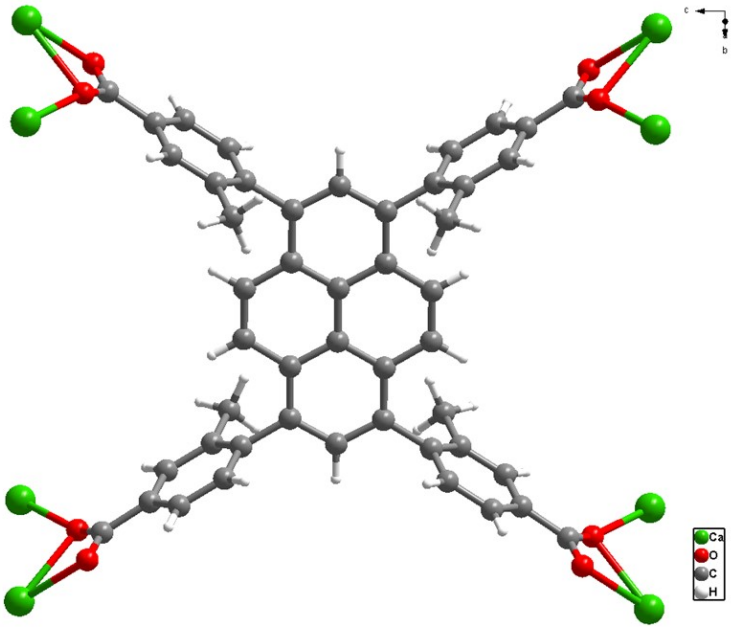

Figure S2. The coordination environment of the independent TCMPP in the crystal structure of HIAM-204

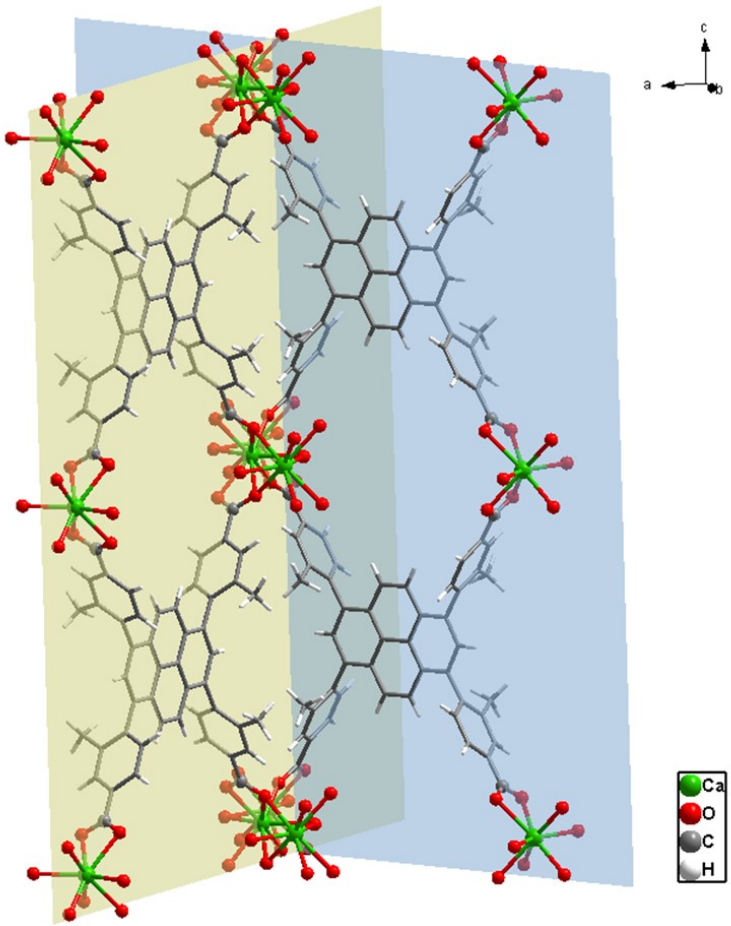

Figure S3. A dihedral angle between the planes of $TCMPP^{4-}$ ligands bound to two subsequent Ca atoms (marked in blue and orange) of 79.29°

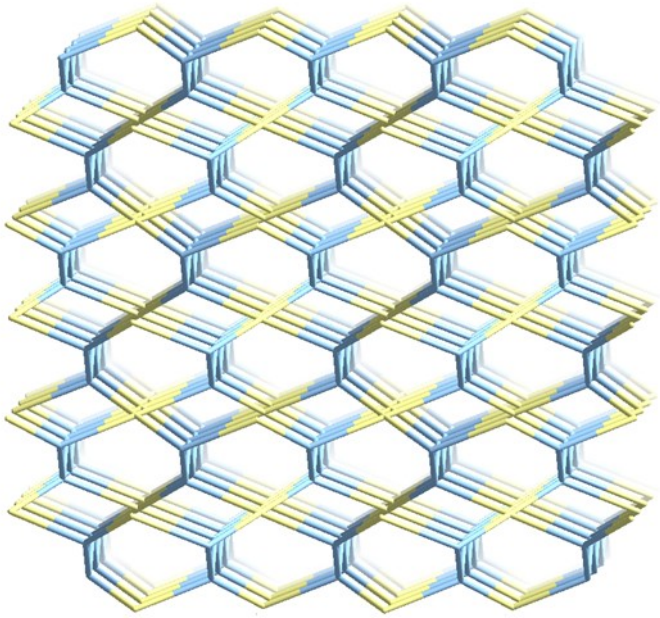

Figure S4. The topological structure of HIAM-204

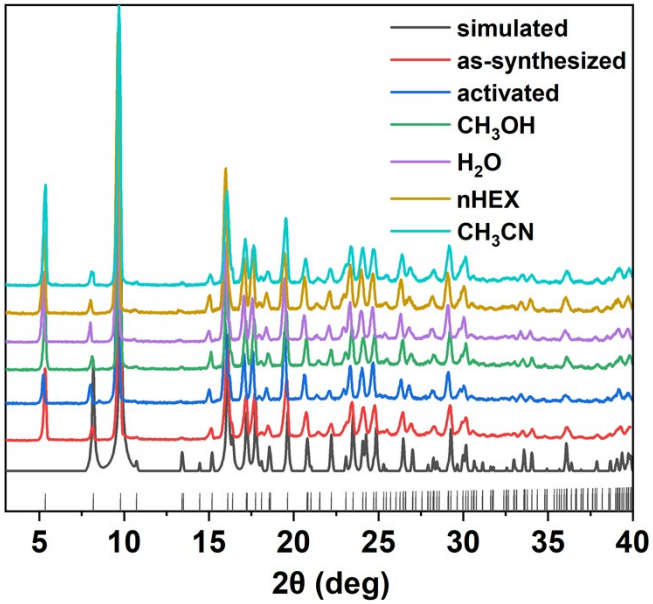

Figure S5. The PXRD patterns of the simulated, the synthesized, activated sample and after being soaked in various organic solvents on HIAM-204

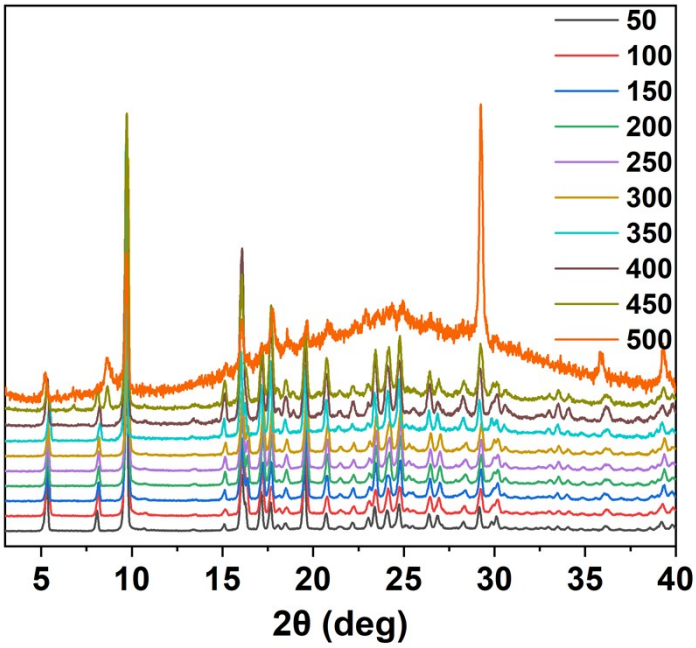

Figure S6. The PXRD patterns of HIAM-204 at different temperatures

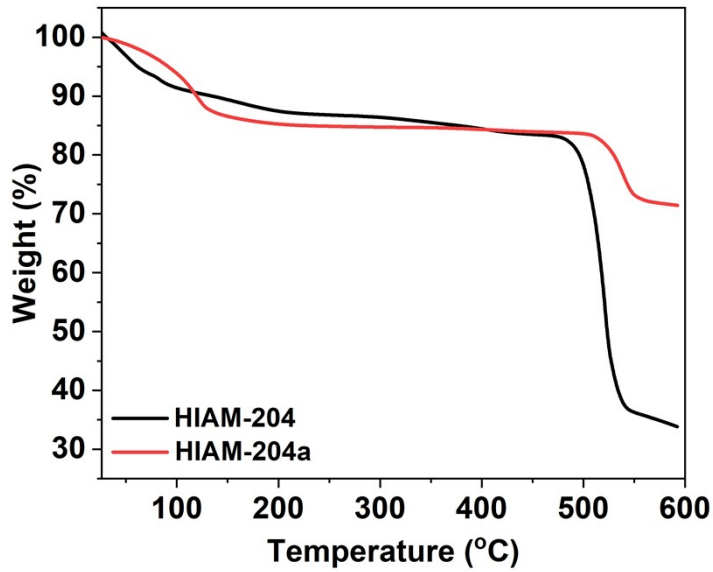

Fig. S7. TG curves of synthesized HIAM-204 and activated HIAM-204a.

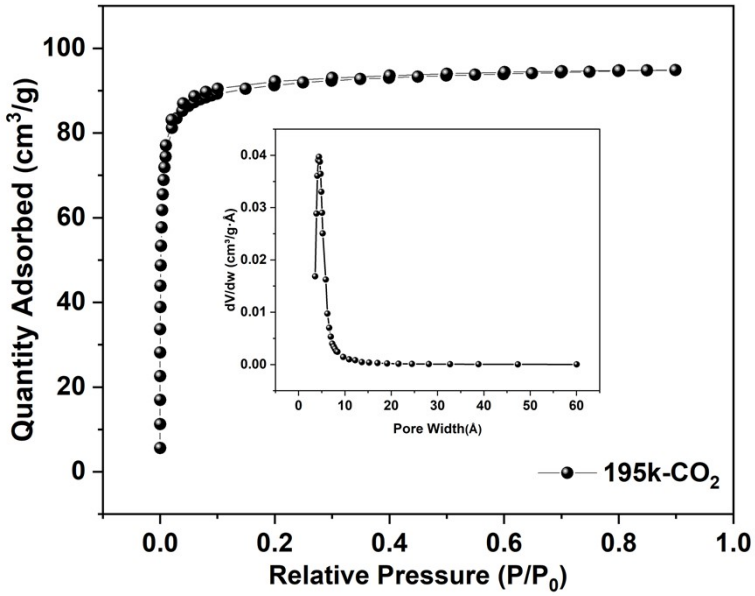

Figure S8. CO_2 adsorption isotherm of HIAM-204 at 195 K and the pore-size distribution for HIAM-204

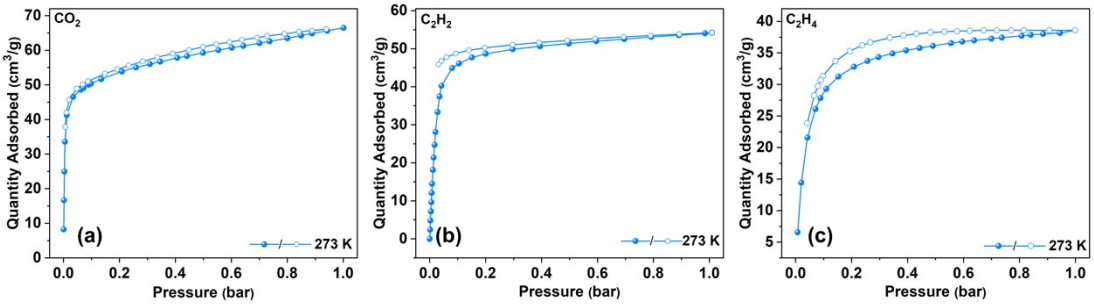

Fig. S9. Adsorption isotherms of CO_2, C_2H_2 and C_2H_4 at 273K by HIAM-204a

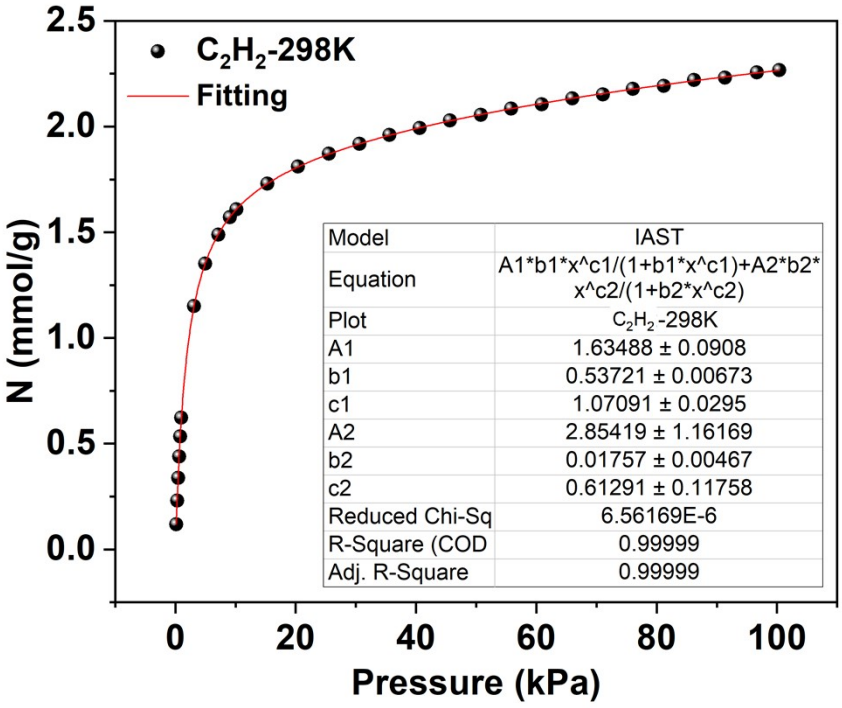

Fig. S10. The Langmuir-Freundlich fittings of C_2H_2 at 298K on HIAM-204

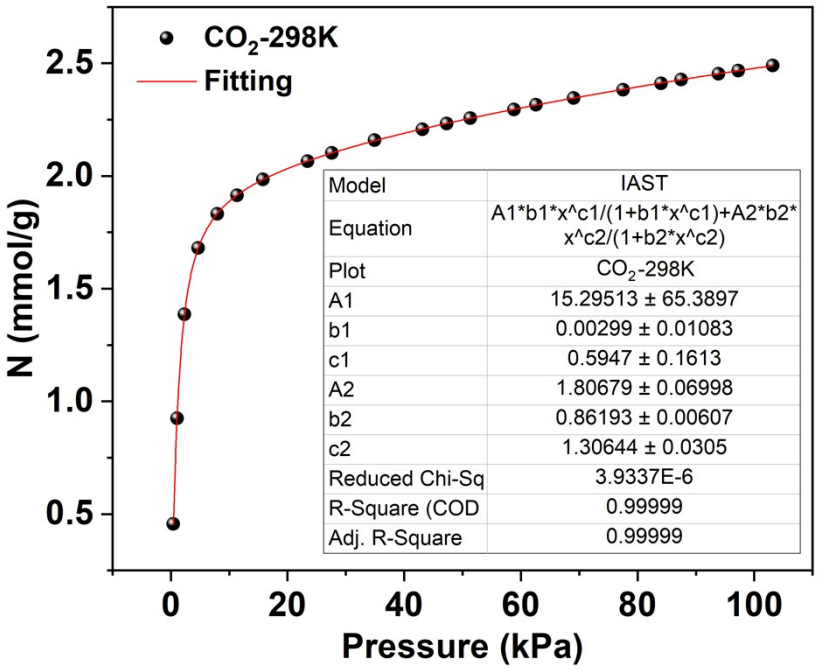

Fig. S11. The Langmuir-Freundlich fittings of CO_2 at 298K on HIAM-204

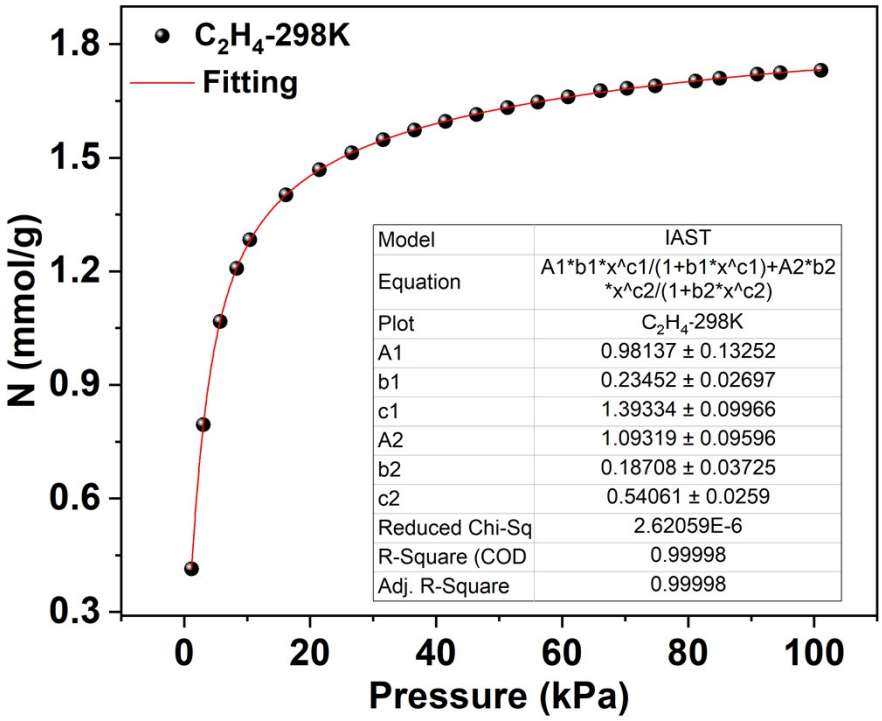

Fig. S12. The Langmuir-Freundlich fittings of C_2H_4 at 298K on HIAM-204

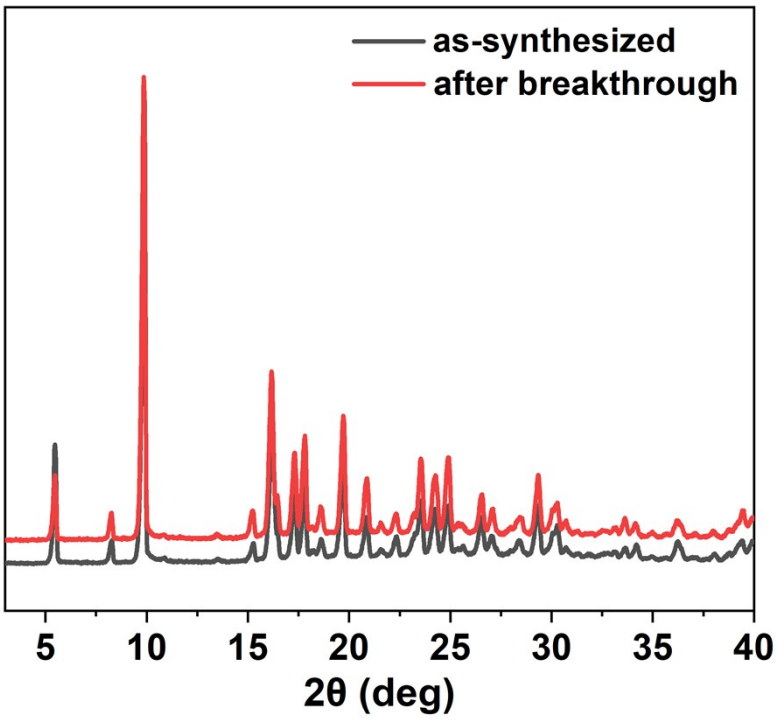

Fig. S13. The PXRD patterns of synthesized and after breakthrough HIAM-204

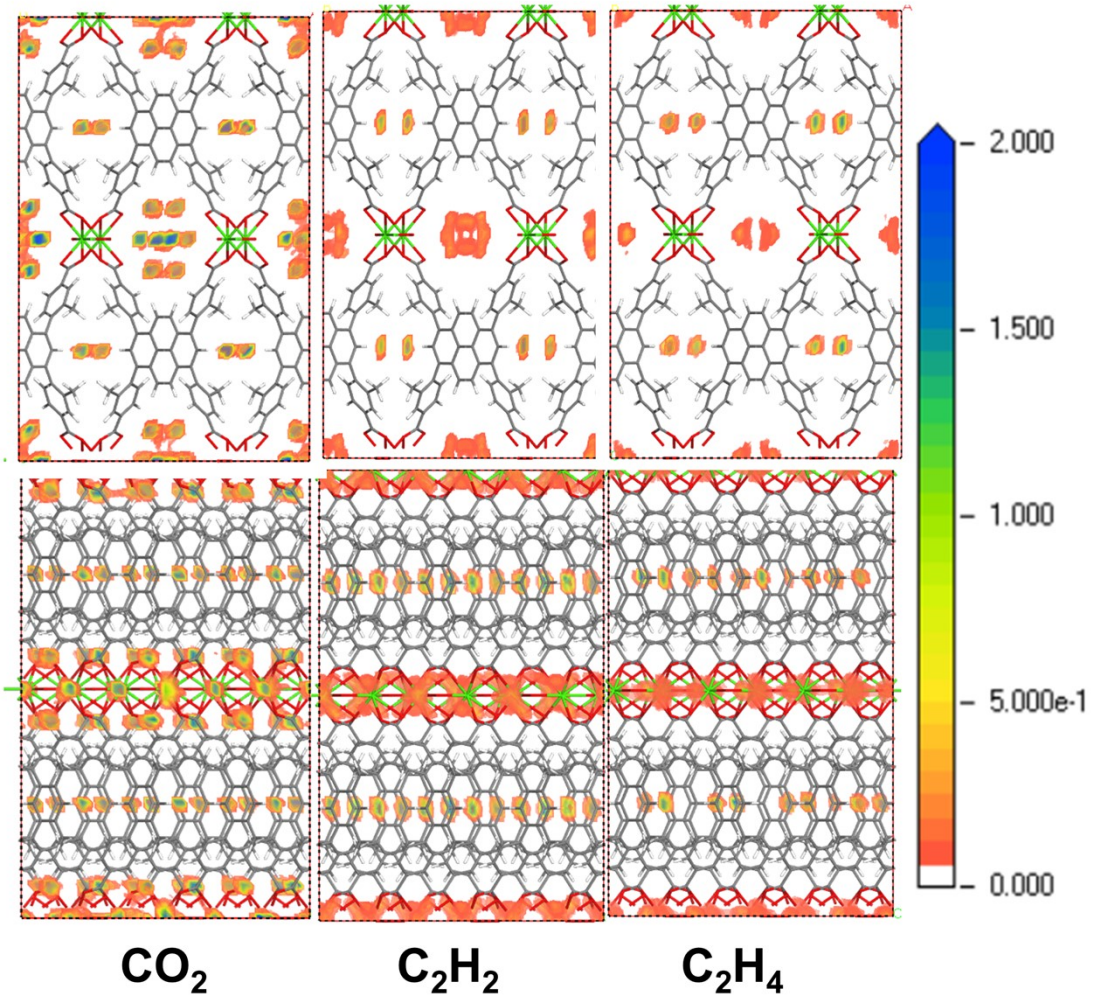

Fig. S14. Computational simulations for the density distribution of CO_2, C_2H_2 and C_2H_4 on HIAM-204 at 1 bar and 298K

Table S1. Crystal data and structure refinements for HIAM-204

MOF	**HIAM-204**
Empirical formula	$C_{24}H_{15}CaO_5$
Formula weight	423.44
Crystal system	orthorhombic
Space group	Pbam
a(Å)	21.598(6)
b(Å)	6.9255(15)
c(Å)	16.482(3)
α(deg)	90
β(deg)	90
γ(deg)	90
Volume (Å^3)	2465.4(10)
Z	4
D_{calc} (g·cm^{-3})	1.141
μ/mm^{-1}	2.432
F(000)	876.0
R_{int}	0.0879
Reflections collected/unique	4659
Data/restraints/parameters	2270/0/144
GOF on F^2	0.997
R_1[a], wR_2[b][$I > 2\sigma(I)$]	R_1 = 0.0805, wR_2 = 0.2065
R_1[a], wR_2[b] (all data)	R_1 = 0.1199, wR_2 = 0.2457
Largest diff. peak/hole /e Å^{-3}	0.44/-0.59

Table S2. Comparison of adsorptive separation properties of HIAM-204 with the adsorbents reported in the literature at 298 K and 1.0 bar.

Adsorbents	CO_2 (cm^3/g) 10 kPa	CO_2 (cm^3/g) 100 kPa	C_2H_4 (cm^3/g) 100kPa	CO_2/C_2H_4 selectivity	Ref.
CALF-20	53.30	78.80	/	/	4
ZnATZox H_2O	51.00	61.90	/	/	5
TIFSIX-3-Ni	49.70	52.00	/	/	6
HIAM-204	42.87	55.79	39.37	5.54	This work
MUF-16	27.78	40.10	/	/	7
SIFSIX-17-Ni	24.00	51.50	4.90	/	8
FJU-44a	15.90	53.20	/	/	9
$In(aip)_2$	7.70	28.10	/	/	10
Qc-5-Cu-sql	14.50	48.40	/	/	11
ZIF-90	4.70	45.00	/	/	12
YZ-6a	4.10	45.30	/	/	13
NTU-67	28.30 (7.5 KPa)	45.70	31.60	10.80	14
UTSA-16	45.00	92.00	52.00	5.70	15
ZNU-6	49.50	106.60	106.00	~4.50	16
5A Zeolite	/	81.00	69.70	2.60	14
NTU-65	2	51.50	26.90	2.50(263 K)	18
CSH-2-700	/	24.60	15.00	1.9	19
TpPa-NO_2	/	45.20	32.50	1.7	20
Zn-atz-oba	/	56.00	45.50	1.23	21
BSF-3	/	47.30	53.10	0.60	22

References

(1) B. Delley. *J. Chem. Phys.*, 2000, **113**, 7756-7764.

(2) J. P. Perdew, K. Burke and M. Ernzerhof, *Phys. Rev. Lett.* 1996, **77**, 3865-3868.

(3) M. Methfessel and A.T. Paxton, *Phys. Rev. B*, 1989, **40**, 3616-3621.

(4) D. A. Kang, N. Suphavilai, A. M. Mohamed, I. G. Economou, M. Shetty, J. Kim, H. K. Jeong, *J. Mater. Chem. A*, 2025, **13**, 18892-18899.

(5) X. Wang, Y. Chen, W. Li, C. Wang, T. Zhao, A. Bakhtiyarovich Ibragimov and J. Gao, *Chem. Eng. J.*, 2024, **498**, 155338.

(6) S. Ullah, K. Tan, D. Sensharma, N. Kumar, S. Mukherjee, A. A. Bezrukov, J. Li, M. J. Zaworotko and T. Thonhauser, *Angew. Chem. Int. Ed.*, 2022, **61**, e202206613.

(7) O. T. Qazvini, S. G.Telfer, *ACS Appl. Mater. Interfaces.*, 2021, **13**, 12141-12148.

(8) S. Mukherjee, N. Kumar, A. A. Bezrukov, K. Tan, T. Pham, K. A. Forrest, K. A. Oyekan, O. T. Qazvini, D. G. Madden, B. Space and M. J. Zaworotko, *Angew. Chem. Int. Ed*., 2021, **60**, 10902-10909.

(9) Y. Ye, H. Zhang, L. Chen, S. Chen, Q. Lin, F. Wei, Z. Zhang, S. Xiang, *Inorg. Chem.,* 2019, **58**, 7754-7759.

(10) Y.-M. Gu, H.-F. Qi, S. Qadir, T.-J. Sun, R. Wei, S.-S. Zhao, X.-W. Liu, Z. Lai and S.-D. Wang, *Chem. Eng. J*., 2022, **449**, 137768.

(11) K. J. Chen, D. G. Madden, T. Pham, K. A. Forrest, A. Kumar, Q. Y. Yang, W. Xue, B. Space, J. J. t. Perry, J. P. Zhang, X. M. Chen and M. J. Zaworotko, *Angew. Chem. Int. Ed*., 2016, **55**, 10268-10272.

(12) H.-F. Zhang, M. Li, X.-Z. Wang, D. Luo, Y.-F. Zhao, X.-P. Zhou and D. Li, *J. Mater. Chem. A*, 2018, **6**, 4260-4265.

(13) D. S. Zhang, Y. Z. Zhang, X. Zhang, F. Wang, J. Zhang, H. Hu, J. Gao, H. Yan, H. L. Liu, H. Y. Ma, L. L. Geng and Y. W. Li, *ACS Appl. Mater. Interfaces*, 2019, **11**, 20104-20109.

(14) Q. Dong, Y. Huang, K. Hyeon-Deuk, I. Y. Chang, J. Wan, C. Chen, J. Duan, W. Jin and S. Kitagawa, *Adv. Funct. Mater*., 2022, **32**, 2203745.

(15) X. Li, Q. Ding, J. Liu, L. Dong, X. Qin, L. Zhou, Z. Zhao, H. Ji, S. Zhang and K. Chai, *Mater. Horiz*., 2023, **10**, 4463-4469.

(16) Y. Jiang, Y. Hu, B. Luan, L. Wang, R. Krishna, H. Ni, X. Hu and Y. Zhang, *Nat. Commun*., 2023, **14**, 401.

(17) Q. Dong, X. Zhang, S. Liu, R. B. Lin, Y. Guo, Y. Ma, A. Yonezu, R. Krishna, G. Liu, J. Duan, R. Matsuda, W. Jin and B. Chen, *Angew. Chem. Int. Ed*., 2020, **59**, 22756-22762.

(18) Z. Zhao, Y. Liu, X. Liu, Y. Liu, J. Chen, S. Chen, S. Deng and J. Wang, *AIChE J*., 2023, **69**, e18046.

(19) X. H. Xiong, L. Zhang, W. Wang, N. X. Zhu, L. Z. Qin, H. F. Huang, L. L. Meng, Y. Y. Xiong, M. Barboiu, D. Fenske, P. Hu and Z. W. Wei, *ACS Appl. Mater. Interfaces*, 2022, **14**, 32105-32111.

(20) J. W. Cao, S. Mukherjee, T. Pham, Y. Wang, T. Wang, T. Zhang, X. Jiang, H. J. Tang, K. A. Forrest, B. Space, M. J. Zaworotko and K. J. Chen, *Nat. Commun*., 2021, **12**, 6507.

(21) Y. Zhang, J. Hu, R. Krishna, L. Wang, L. Yang, X. Cui, S. Duttwyler, H. Xing, *Angew. Chem. Int. Ed.,* 2020, **132**, 17817-17822.